ACS SENSORS

pubs.acs.org/acssensors

Article

Rapid Detection of Circulating Breast Cancer Cells Using a Multiresonant Optical Fiber Aptasensor with Plasmonic Amplification

Médéric Loyez,* Eman M. Hassan, Maxime Lobry, Fu Liu, Christophe Caucheteur, Ruddy Wattiez, Maria C. DeRosa, William G. Willmore, and Jacques Albert

Cite This: *ACS Sens.* 2020, 5, 454−463

Read Online

ACCESS | Metrics & More | Article Recommendations | Supporting Information

ABSTRACT: The detection of circulating tumor cells (CTCs), which are responsible for metastasis in several forms of cancer, represents an important goal in oncological diagnosis and treatment. These cells remain extremely challenging to detect, despite numerous previous studies, due to their low concentration (1−10 cells/mL of blood). In this work, an all-fiber plasmonic aptasensor featuring multiple narrowband resonances in the near-infrared wavelength range was developed to detect metastatic breast cancer cells. To this aim, specific aptamers against mammaglobin-A were selected and immobilized as receptors on the sensor surface. In vitro assays confirm that the label-free and real-time detection of cancer cells [limit of detection (LOD) of 49 cells/mL] occurs within 5 min, while the additional use of functionalized gold nanoparticles allows a 2-fold amplification of the biosensor response. Differential measurements on selected optical resonances were used to process the sensor response, and results were confirmed by microscopy. The detection of only 10 cancer cells/mL was achieved with relevant specificity against control cells and with quick response time.

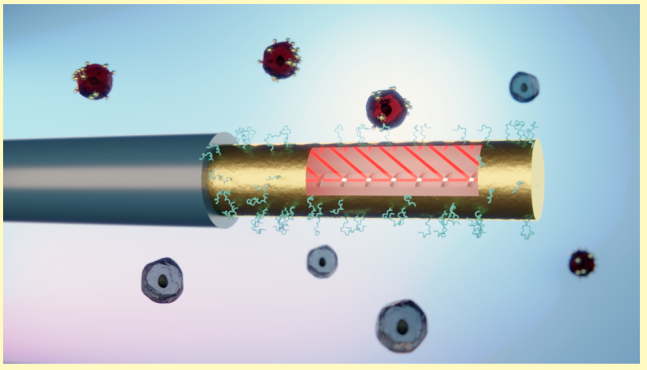

KEYWORDS: *surface plasmon resonance, aptamer, mammaglobin, biomarker, breast cancer cells, biosensing*

Breast cancer is the most common cancer in women. It is also the second global leading cause of cancer death worldwide, closely following lung cancer.[1] The main cause of breast cancer death is in connection with its late diagnosis, often revealing the presence of metastases.[2]

Classical examinations for breast cancer include mammography, magnetic resonance imaging (MRI), ultrasound, or positron emission tomography (PET-scans).[3] On top of these techniques, the early detection of circulating tumor cells (CTCs) in blood consists of an awaited noninvasive diagnosis or prognosis method.[4] It is also a relevant alternative to biopsies, which are still too often required to perform advanced histological analyses. Indeed, the identification and characterization of CTC populations in blood samples are a relevant indicator of breast cancer.[5,6] For the last decade, research has been very fruitful in this area, but the major limitation is still their scarcity (about one CTC for 10^9 hematologic cells in the blood of metastatic cancer patients), imposing the use of high-performance analytical devices.[7]

Among all of the available sensing technologies, surface plasmon resonance (SPR) and localized surface plasmon resonance (LSPR) have been intensively studied for the detection of low-concentrated analytes, especially for medical diagnosis.[8,9] Furthermore, plasmonic features can be tightly exploited with the inherent benefits of optical fibers,[10] bringing miniaturization, flexibility, reliability, remote monitoring, and multiplexing, among others.[11,12] These properties perfectly fit with the aforementioned objective.

The sensitivity enhancement driven by the (L)SPR effects comes from the excitation of free electrons by light on a metal surface.[13] The propagation of the plasmonic wave decreases exponentially at the metal interface and extends evanescently within the surrounding medium, with a depth smaller than the working light wavelength.[14] Different strategies can therefore be considered using optical fibers, such as bent or unclad/etched fibers,[15] long-period fiber gratings (LPFGs),[16,17] or tilted fiber Bragg gratings (TFBGs),[18] to name but a few.

Receptors grafted on top of the metal layer can provide chemical or biological sensing modalities.[19,20] These optical fiber sensors can therefore be considered as miniaturized

Received: November 2, 2019
Accepted: January 22, 2020
Published: January 22, 2020

https://dx.doi.org/10.1021/acssensors.9b02155
ACS Sens. 2020, 5, 454−463

counterparts of the classical SPR devices, such as those relying on the Kretschmann prism. The wide variety of configurations makes it a versatile platform for biochemical sensing.[21,22]

These features allow a fine label-free and real-time monitoring of the binding events taking place on the fiber surface. Hence, plasmonic optical fiber sensors have already proven their legitimacy for medical applications and the detection of analytes at very low concentrations.[23,24] Recent advances in plasmonics have also highlighted the wide extent of concrete bioapplications involving different types of optical fiber sensors. These have been used in the frame of the detection of small molecules in milk,[25] urine,[26] serum, or whole blood,[27] and more recently in resected cancerous human tissues.[28,29] These considerations are particularly relevant for CTC sensing since their presence at low concentration makes sample enrichments and labeling almost always mandatory. Moreover, the convenient sizes of optical fibers allow their use in small volumes, limiting the need for the collection of large samples.

To detect breast tumor cells, the biochemistry performed on our gold-coated optical fibers was refined and involves the immobilization of thiolated aptamers, specifically designed and selected against mammaglobin proteins.[30] These mammaglobin proteins are members of the uteroglobin protein family and are diagnostic biomarkers for breast cancer.[31,32] As they are present at the surface of CTCs shed from a primary tumor and freely circulating in the blood, they are perfectly suited to being targeted with our probes.[33]

To do so, aptamers were used as receptors on the sensor surface. Aptamers are short single-stranded DNA or RNA (or synthetic XNA molecules) with high affinity and specificity for a selected target.[34] Their stability (pH variations, temperature changes, resistance to proteases and lyophilization, etc.) and their long shelf life are some of their many advantages, which make them increasingly exploited in biosensing, also as an alternative to antibodies.[35]

When aptamers recognize their respective targets, the interaction between both molecules induces a local variation of the refractive index at the metal surface. As the surface plasmon wave relies on propagation along that metal surface, the resonance wavelength and the resonance amplitude are impacted and shift proportionally to the refractive change induced by the biomolecules.[36]

In this article, we present an aptamer-based approach to spot breast cancer cells at very low concentrations. We describe the surface biochemistry, specifically designed for the detection of CTC-surface biomarkers. Sensing results were obtained using different cell lines to demonstrate the intrinsic capabilities of the Bragg gratings for specific biodetection. The detection threshold was drastically improved using functionalized gold nanoparticles playing the role of amplification labels, as they interact with the target cells. This experimental study is finally consolidated by a thorough signal demodulation, as well as the microscopic surface analysis.

MATERIALS AND METHODS

Materials. Phosphate buffer saline (PBS) came from Thermo Fisher Scientific (Waltham, MA). Gold nanoparticles (10 nm) and 6-mercapto-1-hexanol were purchased from Sigma-Aldrich (St Louis, MO). All DNA bases and thiol modifiers used in this study were ordered from Glen Research (Sterling, VA). All cell lines were purchased from American Type Culture Collection (ATCC) (Manassas, VA). Cell medium [Dulbecco's modified Eagle's medium (DMEM)] for MDA-MB-415 and HEK293 cells was obtained from Gibco/Thermo Fisher Scientific (Canada). Recombinant human insulin was ordered from Santa Cruz Biotechnology Inc. (Dallas, TX). Mammary epithelial cell growth medium (MEGM) and MEGM kits for MCF10A were purchased from Lonza (Alpharetta, GA).

Aptamer Selection and Synthesis. The used aptamers (MAMA2) were previously selected by Hassan et al.[30] Briefly, the hybrid systematic evolution of ligands by exponential enrichment (SELEX) approach was used. MAMA2 aptamers were selected from a random library containing many sequences of ssDNA. The selection was designed to enrich the ssDNA library toward the mammaglobins by applying a protein SELEX as an initial step and then transferring the enriched library to perform SELEX on breast cancer cells (MDA-MB-415 as a target for the MAMA protein). After rounds of ssDNA library incubation with the target proteins/cells (partitioning off the unbound sequences and amplifying the bound sequences), sequencing was applied to identify the aptamer candidates. MAMA2 was found to have the best affinity toward MDA-MB-415 and was therefore chosen for further studies. Thiolated MAMA2 was synthesized by a MerMade 6 automated DNA synthesizer (BioAutomation) using phosphoramidite chemistry as the standard method of synthesis.[37] The following DNA sequence was used: MAMA2: 5′-CAT GCT TAC CTA TAG TGA ACC CGG GAC AGA ACG TGC GCT TTG AGC TTT GAG AAC TGA CTC ATA C-C-6-S-S-3′.

Cell Cultures and Fixation. MCF7, MDA-MB-415, and HEK293 cells were cultured in DMEM. Human recombinant insulin (0.01 mg/mL) was added as a supplement to only MCF7 and MDA-MB-415 breast cancer cells. Fetal bovine serum (FBS; 10%) was added to the media of all of the above cell lines. For MCF10A cells, they were cultured in the mammalian epithelial cell growth medium kit. All cells were cultured in 5% CO_2, a 95% humidified chamber at 37 °C.

All cells mentioned above were grown in a monolayer for at least 48 h. They were then harvested using 1× trypsin as follows: cells were washed in PBS twice and incubated with 1× trypsin for less than 5 min to detach from the flask. They were then collected in a 15 mL falcon tube and centrifuged at 200 g for 5 min. This process is widely used to ensure that the surface receptors on the cells are still intact. The cells were fixed in a 4% formaldehyde solution in PBS for 15 min at room temperature (RT). The cells were then centrifuged at 1000*g* for 5 min and resuspended in 1 mL of PBS for the SPR analysis. The cells were counted using a hemocytometer to obtain 10^6 cells/mL for each cell line. For detection experiments and calibration curves, a serial dilution of the main stock (10^6 cells/mL) of each cell line was applied.

Tilted Fiber Bragg Grating Inscription and Gold Film Deposition. The tilted fiber Bragg gratings were manufactured using the phase-mask technique. The NORIA manufacturing system (Northlab Photonics, Nacka, Sweden), embedding a deep ultraviolet-pulsed excimer laser (Coherent Excistar XS 500 Hz-Argon Fluor at 193 nm), was used with a phase mask of 1100 nm period and an 8° tilt angle. The tilted gratings were inscribed into the hydrogenated SMF-28 (Corning Inc., Corning, NY), a single-mode silica optical fiber with a diameter of 250 μm (with the polymer jacket) and a core of 8 μm. After the inscription, a ∼50 nm gold film was deposited by evaporation on both sides of the optical fiber grating. The gold coating thickness was verified by atomic force microscopy (AFM).

Biofunctionalization. MAMA2 was reduced using 10 mM Tris-(2-carboxyethyl)-phosphine (TCEP) for each 10 μM of the aptamer. Briefly, 10 μM of MAMA2 was mixed with 10 mM of TCEP in PBS (total volume 100 μL) at RT for 60 min. Then, the excess TCEP was washed using amicon ultracentrifugal filters (0.5 mL, Millipore, Canada), with centrifugation at 10 000 rpm for 20 min, three times. After that, the MAMA2 aptamer was resuspended with 1 mL of PBS to be used for the immobilization step.

The reduced MAMA2 5′-thiolated aptamers (10 μM) were immobilized on the gold-coated gratings in 500 μL of PBS for 1 h at RT. The passivation process was performed after the bonding of the aptamers in PBS using 6-mercapto-1-hexanol 5 mM for 30 min at RT (volume 500 μL). The solutions were freshly prepared before each experiment.

https://dx.doi.org/10.1021/acssensors.9b02155
ACS Sens. 2020, 5, 454−463

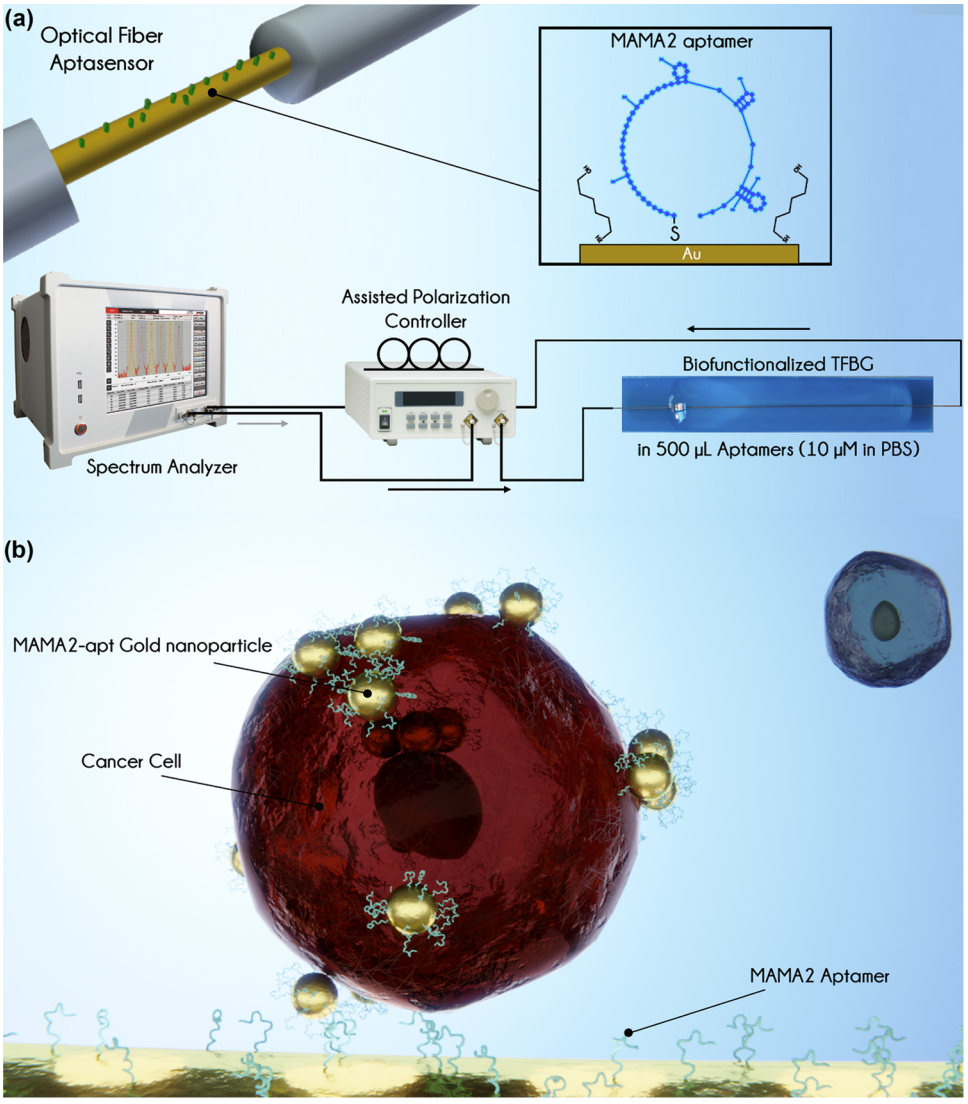

Figure 1. (a) Presentation of the experimental setup, using gold-coated TFBGs biofunctionalized with thiolated aptamers and blocked with mercaptohexanol. The optical fiber is connected to a spectrum analyzer and a polarization controller. Liquid samples are added to the sensing area into a low-bind gut container to ensure total immersion of the grating while limiting the needed volumes to 500−800 μL. (b) Artistic view of the target cancer cells interacting with aptamers (the same MAMA2 aptamers) immobilized on the optical fiber surface and functionalized gold nanoparticles (representation not to scale).

Gold Nanoparticle Functionalization (GNP). Commercial 10 nm gold nanoparticles were used. Thiol-terminated aptamers (10 μM) were incubated with 1.5 mL gold nanoparticles for 1 h at RT under stirring. The particles were rinsed and blocked with mercaptohexanol (5 mM) for 30 min. After the reaction, they were washed and finally centrifuged to remove the supernatant and were resuspended in PBS buffer. The particles were freshly prepared prior to each experiment to avoid precipitation or the formation of clusters due to the buffers.

Interrogation Setup and Data Analyses. The biofunctionalized biosensors were connected in transmission to a light polarization controller (MPC-201, General Photonics, Chino) and to a spectrum analyzer (OSA20 Yenista Optics, EXFO America Inc., Richardson). The sensing area was kept straight between two clamps in a small gutter used to apply the functionalization solutions, and the samples were tested in small volumes, ranging from 500 to 800 μL, covering more than the whole TFBG area (~1.5 cm) (Figure 1a). The solutions were all prepared in low-bind containers. The experiments were conducted in those conditions with cells without gold nanoparticles (GNPs) and after the addition of functionalized gold nanoparticles as amplification labels (Figure 1b).

The experimental data were acquired automatically with home-developed monitoring software. The data were then analyzed using Origin 9.0 (OriginLab, Northampton) and MATLAB (MathWorks, Natick), according to the performed analyses. Statistical analyses were conducted with R-studio (Open Source Edition, Boston).

The theoretical calculation of the limit of detection (LOD) was based on the method recommended by the IUPAC in analytical chemistry, which is defined as the lowest quantity of a substance that can be distinguished from the absence of that substance (blank) with a stated confidence level (>99%). The calculation is based on 3 times the standard deviation (σ) of the blank, reported on the experimental calibration curve at low concentrations. As we considered the use of nontarget cells as negative controls, we have taken into account the signal variations in a nonspecific medium as the worst-case situation to increase the reliability of the LOD calculation.[38,39]

RESULTS AND DISCUSSION

Validation of the Biosensor Functionalization Process. Gold-coated TFBGs immersed in PBS show singular spectral features arising from the excitation of an SPR on the

https://dx.doi.org/10.1021/acssensors.9b02155
ACS Sens. 2020, 5, 454−463

outer surface of the metal coating. This coupling results in the attenuation of the cladding-mode resonances within a narrow spectral region where the SPR is excited. There is, consequently, a decrease in their amplitudes, as shown in the shaded area of the transmission spectrum (Figure 2a). Resonances further away from the SPR become increasingly less sensitive, up to a core-mode resonance at the so-called Bragg wavelength, located at the right end of the spectrum.

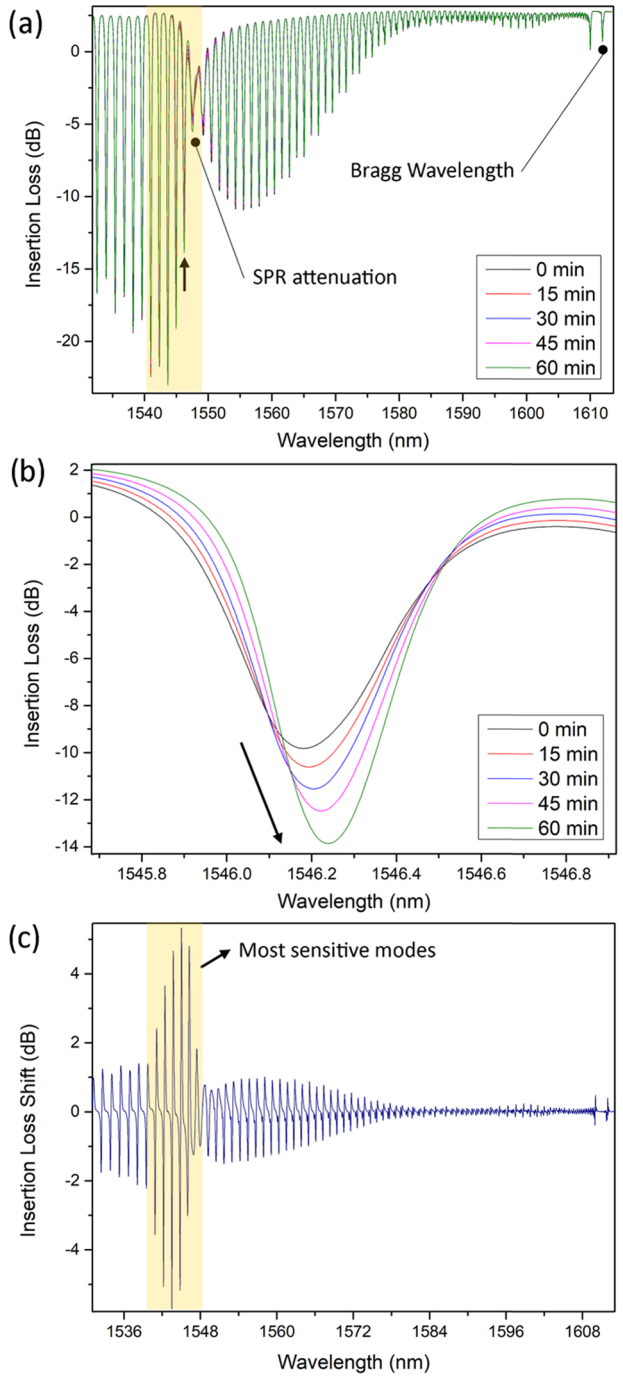

Figure 2. (a) Superposition of the spectra obtained with gold-coated TFBGs in the aptamer solution during the biofunctionalization process lasting 1 h. (b) Zoom on the sensitive-mode resonance indicated by an arrow in 2a. (c) Difference between the spectra obtained after and before functionalization to localize the most sensitive-mode resonances.

The latter can be used to compensate for room-temperature fluctuations by shifting the spectra to line up their Bragg wavelength to a fixed value.[18]

Because of the high dispersion of the SPR with respect to the permittivity of the medium immediately adjacent to the metal surface, near-infrared (NIR) resonances located closest to the SPR attenuation show the highest sensitivity (Figure 2b), while others are increasingly less impacted by the surrounding refractive index changes. By subtracting the spectra obtained at the end of the functionalization process from those obtained in the reference PBS solution at the beginning of the experiment, we could elucidate that the most sensitive modes are located on the short wavelength side of the maximum SPR attenuation but not immediately within the SPR maximum so as to be too attenuated (Figure 2c). Using this technique, we refined the positioning and automatic selection of the most sensitive mode for the biosensing analysis in any gold-coated TFBG.

Spectral Sensitivity Analysis. A closer analysis of the spectral changes observed in the vicinity of the SPR attenuation in our gold-coated TFBGs shows signal evolutions that are exceptionally clear and that perfectly fit the expected theoretical behavior of the SPR sensing properties. In particular, the nearest-neighbor resonances on each side of the SPR maximum attenuation wavelength become less attenuated on the short wavelength side and more attenuated on the long wavelength side, as the SPR shifts to longer wavelengths in response to a refractive index increase near the surface of the gold-coated TFBG following the binding of receptors (Figure 3a). A comparison between the sensitive modes closest to the SPR region (labeled SPR −1 and SPR +1) during aptamer immobilization clearly shows this expected trend (Figure 3b), a trend that is a universal feature of gold-coated TFBGs in the SPR conditions.[40,41] For accurate biosensing, however, the second nearest resonance on the short wavelength side generally provides better sensitivity, in view of its larger initial amplitude and location on the high slope of the SPR attenuation (the resonance used for Figure 2b is also an SPR −2). It is further possible to compare shifts between the SPR-sensitive and SPR-insensitive resonances in a given biosensing experiment. This is achieved using the self-referenced analysis, which ensures a high level of confidence for the variations of both the wavelength and amplitude of the most sensitive resonances. This is particularly evident during the biofunctionalization measurements shown in Figure 3c,d over a period of 60 min. In the remainder of this paper, amplitude change results will be used exclusively because their signal-to-noise ratio is much higher: while the power level noise floor for these experiments is ∼40 dB below the signal traces shown, the total wavelength shifts of the resonances (a few tens of picometers) are not much larger than our statistically determined measurement accuracy of ∼2 pm.

Cell Detection Using TFBG Aptasensors. Thiolated molecules, such as our SH-terminated aptamers, can easily bind to gold surfaces. Thanks to the generation of SPR in PBS buffer, we were able to track the functionalization process in real time (Figure 4a). According to the literature, we tested different incubation times, ranging from 45 min to 2 h, and we observed a significant signal shift as a function of the immobilization time, with a lower immobilization rate after 1 h (Figure S1). This was therefore considered as the more optimized incubation time for our experimental process.[40]

https://dx.doi.org/10.1021/acssensors.9b02155
ACS Sens. 2020, 5, 454−463

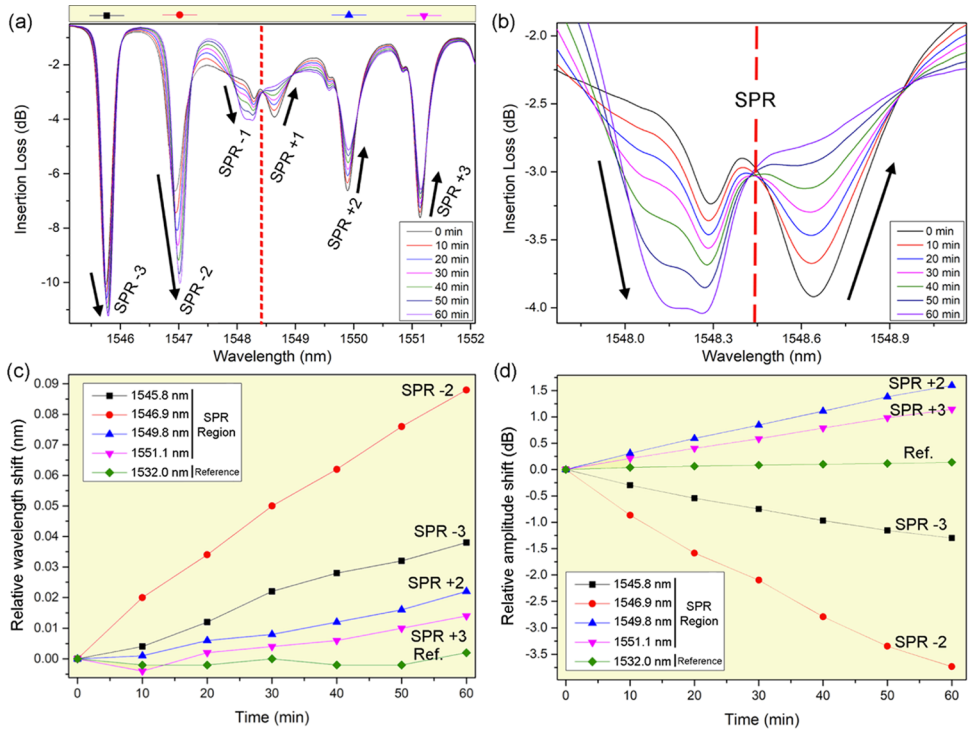

Figure 3. (a) Spectral evolution near the SPR attenuation over 60 min of the aptamer immobilization (labels refer to the numbering convention used to identify sensitive modes in the TFBG-SPR spectra). (b) Evolution of the most attenuated mode resonances. (c) Evolution of the center wavelengths of resonances near the SPR maximum, with respect to their starting value (the resonance identified by "ref" is located at 1532 nm, corresponding to SPR −12). (d) Evolution of the minimum power level of the same resonances with respect to their starting value.

After the aptamer binding, passivation was performed using a 5 mM 6-mercapto-1-hexanol solution to block any possible remaining surfaces that were not functionalized by the aptamers. It appears that the blocking was efficient, and it was also monitored with lower shifts than those observed for the functionalization process, reaching saturation 15−20 min after immersion (Figure S2).

The sensors show interesting features in terms of specificity. When adding 100 MCF10A (negative control) cells onto the TFBG surface, there was no difference between the spectra in PBS after and before the addition of the cells. However, it is important to mention that few unspecific interactions can be observed during the experiments, due to the deposition of some cells by gravity from the buffer to the optical fiber surface. To avoid these nonspecific detections, we realized that the use of the sensor positioned halfway up the cylindrical gutter recipient can limit this phenomenon (Figure S3). Many biosensors are using microfluidics systems to bring the samples into contact with the sensor surface. However, this often implies the use of larger sample volumes and consequently brings complexity to the system. As we want to detect cells in the simplest way and with small volumes, we tried to target the cells into a drop of the buffer, while the initial pipetting ensures sufficient homogenization of the solution to resuspend the cells within the detection time.

We determined that the kinetics of the cell interactions with the TFBG occurs within 10 min, with higher impacts on the signal responses during the first 5 min (Figure 4b). As mentioned earlier for the functionalization process, the use of self-reference cladding modes is needed to verify the stability of the fibers and to ensure that the variations are exclusively related to SPR shifts (Figure 4c).

The use of control cells at high concentrations (10^4 cells/mL in PBS buffer) pinpoints a high stability of the system, while the addition of a limited number of target cells (100 cells/mL in PBS buffer) exhibits a significant variation of the sensing response, according to the results obtained from six independent optical fiber biosensors (Figure 4d). The variations were tested after washing using 1 mL of PBS and after 2 min of signal stabilization. The difference between the fiber response in PBS before and PBS after the presence of 100 target cells/mL is presented in Figure 4e. The biosensing curve obtained with these target cells at low concentration is significantly higher than the signal threshold obtained with a higher number of control cells (p-value = 0.013). Statistical analyses were performed on the data to determine the significance of the results (Figure S4). These control cells were used to check the specificity of the probe, prior to the addition of target cells. The cell sizes and characteristics are known to be different if the cells are tumoral or healthy. They can also show very different parameters in terms of size or composition. The inherent properties of CTCs can explain the variability of the sensing response, depending on how the cells attach to the surface and if they are larger or smaller. For instance, MCF10A present sizes between 678 and 1317 μm^3. These are close to the HEK cells that are around 1406 μm^3. The target MDA cells used are comparable in size to these normal cell lines.[42,43]

Analysis of the Optical Fiber Surface. To confirm the correct bonding of receptors on their gold-coated surface, optical fibers were functionalized with fluorescently tagged aptamers and observed through microscopy (Figure 5a−c). The presence of aptamers was highlighted through the green fluorescence while negative controls exhibited no signal. The interactions of cells with the optical fiber surface were also

https://dx.doi.org/10.1021/acssensors.9b02155
ACS Sens. 2020, 5, 454−463

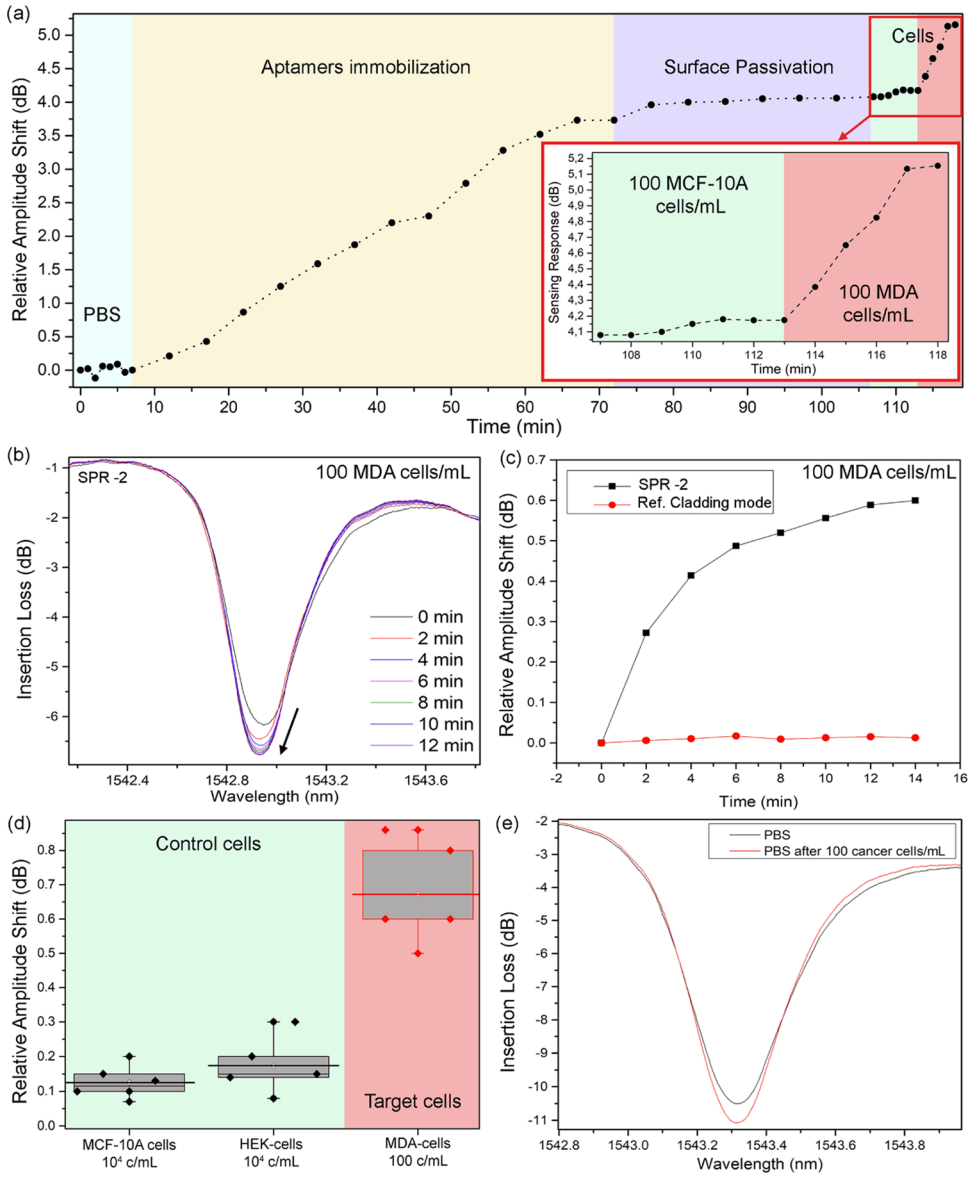

Figure 4. (a) Sensorgram showing the functionalization process, blocking and detection steps in real time. The analysis was performed in PBS, thiolated MAMA2 aptamers, blocking agent, control cells (100 c/mL), and target cells (100 c/mL) shown in the enlarged graph area. (b) Evolution of an SPR-sensitive mode during target cell binding over 12 min. (c) Measured shifts show that most of the interactions occurred within 5 min, with signal stabilization after 10 min. (d) Boxplot of the biosensing shifts in PBS after MCF10A control cells (10^4/mL), PBS after HEK control cells (10^4 c/mL), and PBS after 100 MDA target cells/mL ($N = 6$, p-value = 0.013, R-studio v1.0.153). (e) Zoom on the sensing mode recorded in PBS before and after 100 MDA target cells/mL detection.

verified using two techniques: microscopy under visible light and scanning electron microscopy (SEM).

The SEM analysis of cells needs a second gold deposition to verify their presence and preserve their integrity as the vacuum can provoke damage. After a thin additional gold deposition on top of the optical fiber surface, we managed to observe the immobilized cells (Figure 5d).

This experiment was confirmed by the monitoring of cell interactions with the sensor surface during their addition at a concentration of 1000 c/mL using visible microscopy in a liquid medium (Figure 5e). The focus on both the cells and optical fiber is challenging due to the measured depth of the field. It is possible to overcome this by playing with the reflection of light and by working on a semitransparent holder, on which the optical fiber and the liquid sample are added. It is important to mention that the power of the light source can quickly evaporate the solutions. It is therefore important to immerse the fiber in a sufficient volume while limiting the depth of the selected container.

Functionalized Gold Nanoparticles as a Signal Amplification Label. The direct, label-free detection of cells was achieved at different concentrations. According to the experimental results, detections were obtained from 100 cells/mL, which remains a very low experimental threshold but is not enough, given the target application (calculated LOD of 49 cells/mL) (Figure S6). Some of our most sensitive probes showed interesting behaviors while adding only 10 or 50 cells per mL, but the responses achieved yielded poor signal-to-noise ratio. Hence, we investigated the possibility to reach lower cell concentrations through the use of the gold nanoparticles amplification.

https://dx.doi.org/10.1021/acssensors.9b02155
ACS Sens. 2020, 5, 454−463

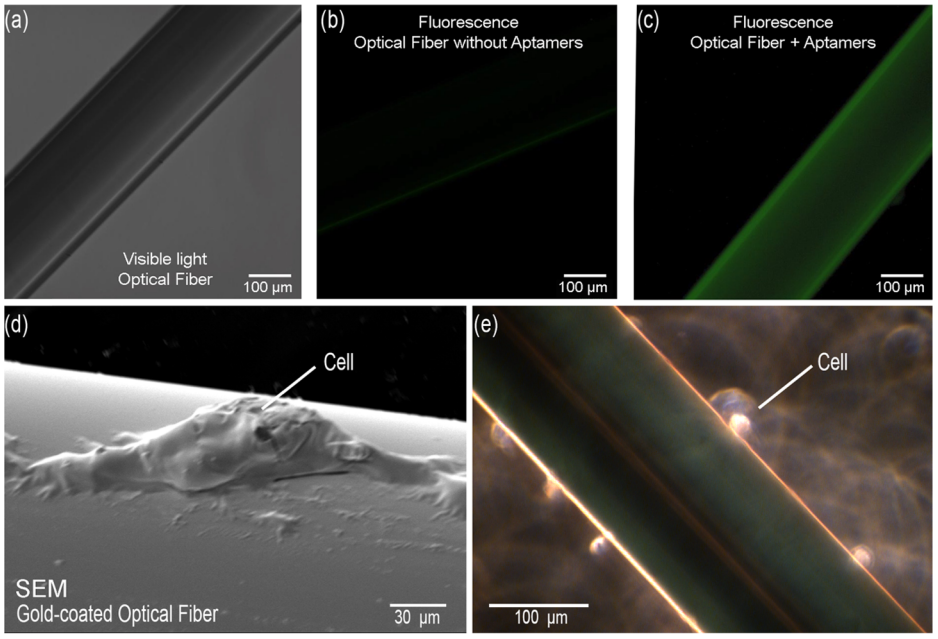

Figure 5. Confocal microscopy analysis of the optical surface. (a) Observation of the gold-coated TFBG in visible wavelengths. (b) Negative control using fluorescence mode with a gold-coated TFBG without the aptamer immobilization. (c) Fluorescence revealing the presence of labeled aptamers in green on a gold-coated TFBG. (d) SEM images of cell interactions with the fiber surface. To perform the SEM analysis, a second gold deposition was needed after detection to obtain images of the cells (×1300). The vacuum and the gold deposition can affect the shape and the size of the immobilized cells. (e) Interactions between cells and a biofunctionalized optical fiber under a microscope, in spiked PBS buffer (×100).

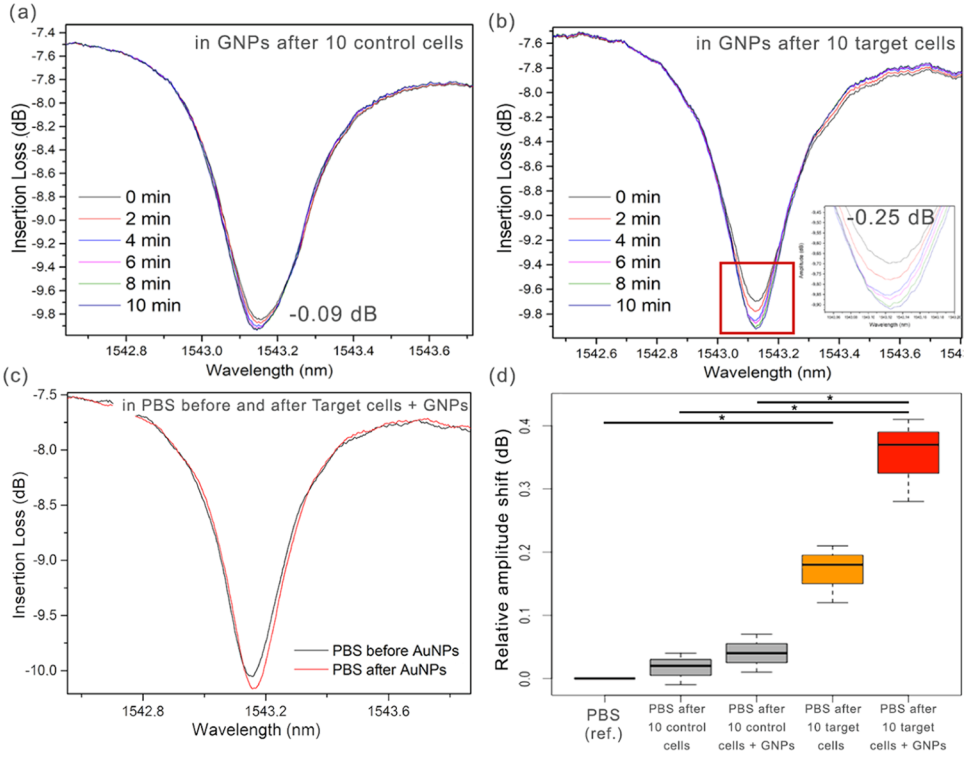

Figure 6. (a) Evolution of the signal in the functionalized gold nanoparticle solution after 10 control cells/mL. (b) Evolution of the signal in the functionalized gold nanoparticle solution after 10 target cells/mL. (c) Signal variation in PBS before and after the addition of MAMA2-GNPs after the 10 target cells/mL incubation. (d) Boxplot of the relative amplitude shift in PBS (ref) and after each tested condition ($N = 3$, p-value <0.05, R-studio v1.0.153).

To appreciate the fair value of these results, let us recall that the cells are the smallest units of living organisms while being among the largest elements in the world of the infinitely small. It is well known that SPR is suitable for small biomolecule sensing,[44] but it is also a technique of interest for cell detection.[45,46] We have already demonstrated that the penetration of the evanescent wave into the external medium while using gold-coated TFBGs in the NIR is around 700−800

https://dx.doi.org/10.1021/acssensors.9b02155
ACS Sens. 2020, 5, 454−463

nm, according to the experimental setup used.[41] This means that the sensing area with cells is only located on a part of the membrane interacting with the fiber surface. As the covered area and the mass effect of the cells are much higher than with the free circulating proteins, we believe that the impact of the refractive index (RI) change is locally higher. As such, the detection can occur with only a low number of hits on the surface, while a global effect is needed for the small biomolecule detection, all over the sensing area. This phenomenon probably explains why the sensitivity threshold can be different from one target to another.

To increase the signal-to-noise ratio and to lower the cell detection threshold obtained with the previously described label-free detection, we functionalized 10 nm gold nanoparticles (GNPs) with the same thiolated MAMA2 aptamers that were used on the sensor surfaces. This means that MAMA2-GNPs will be able to bind the free surface proteins on the cells, the latter previously attached to aptamers on the SPR-TFBG by some of the target proteins close to the gold surface. These GNPs were then implemented as amplification labels at the end of the detection experiments (Figure 6a). The use of GNPs as biosensing enhancers is a well-known technique. Their presence on top of the immobilized targets will have two main effects. The first will be a chemical enhancement due to their nature (mass effect, local refractive index change, etc.). The second will be an electromagnetic field enhancement yielding higher sensitivity.[47,48] This is only true if the gold nanoparticles are located within the range of the evanescent wave into the external medium, as mentioned above. Only a few nanoparticles immobilized on the closest parts of the target cells will therefore play the role of enhancers, while the others will not have any effect.

The recordings performed during the addition of MAMA2-GNPs showed small shifts related to the unspecific adsorption on control probes (Figure 6a) and were avoided by the washing step (1 mL PBS) after incubation. Higher shifts were observed while adding MAMA2-GNPs on the target cells, immobilized on the sensors (Figure 6b). These shifts were both higher during the GNP immobilization and after the washing steps, yielding a detection of 10 target cells/mL in PBS (Figure 6c). As the sensing shift before and after the 10 cancer cells incubation was low (around 0.1 and 0.2 dB, relative amplitude shift), the implementation of GNPs successfully improved the signal change and, consequently, the experimental detection threshold (Figure 6d). The use of GNP amplification is essential to stay higher than the noise level, which is particularly relevant if this technique is further implemented on the portable equipment for field measurements, with a lowered signal-to-noise ratio. A statistical analysis (Figure S5) was performed on the detection data obtained from three different SPR-TFBGs successively immersed in the 10 control cells, GNPs, 10 target cells, and GNPs.

CONCLUSIONS

The detection of tumor cells is a hot topic for the development of accurate and highly sensitive diagnostic tools. In this paper, we present the use of specific aptamers directed against mammaglobin proteins, located at the surface of circulating breast cancer cells. Optical fiber grating sensors were functionalized using aptamer receptors to detect cells at low concentrations *in vitro*. An experimental detection reaching 100 cells/mL was achieved with a label-free detection strategy (calculated LOD of 49 cells/mL), while the detection of only 10 cells/mL was observed using gold nanoparticles as a signal amplification tool. A thorough microscopic analysis of the fiber grating surface was performed to validate the functionalization steps and to visualize the interactions between the sensor and the target cells. The specificity of the probes was tested with high concentrations of different cell lines, such as HEK cells, which do not express MAM proteins. The original demodulation techniques were developed to locate the most sensitive modes of light and to exploit the performances of the spectral responses experimentally obtained at their highest degree. These encouraging results demonstrate the relevance of optical-fiber-based sensors for the detection of cells at low concentration and especially in the frame of the early-stage metastatic cancer diagnosis. This finally offers a wide range of possibilities for the future development of SPR-based aptasensors.

ASSOCIATED CONTENT

Supporting Information

The Supporting Information is available free of charge at https://pubs.acs.org/doi/10.1021/acssensors.9b02155.

Aptamer immobilization time (relative amplitude shift during the aptamer immobilization); blocking step efficiency (zoom on the sensitive mode of SPR-TFBG before and after blocking, in PBS buffer); picture of the sample container (gutter) for optical fiber biosensing; details of the LOD calculation; details of the statistical analyses performed on the experimental biosensing results (PDF)

AUTHOR INFORMATION

Corresponding Author

Médéric Loyez − *Proteomics and Microbiology Department, University of Mons, 7000 Mons, Belgium;* orcid.org/0000-0001-8858-7413; Email: mederic.loyez@umons.ac.be

Authors

Eman M. Hassan − *Institute of Biochemistry, Carleton University, Ottawa K1S 5B6, Canada*

Maxime Lobry − *Electromagnetism and Telecommunications Department, University of Mons, 7000 Mons, Belgium*

Fu Liu − *Department of Electronics, Carleton University, Ottawa K1S 5B6, Canada*

Christophe Caucheteur − *Electromagnetism and Telecommunications Department, University of Mons, 7000 Mons, Belgium;* orcid.org/0000-0002-6453-6790

Ruddy Wattiez − *Proteomics and Microbiology Department, University of Mons, 7000 Mons, Belgium*

Maria C. DeRosa − *Institute of Biochemistry, Carleton University, Ottawa K1S 5B6, Canada;* orcid.org/0000-0003-1868-6357

William G. Willmore − *Institute of Chemistry, Carleton University, Ottawa K1S 5B6, Canada*

Jacques Albert − *Department of Electronics, Carleton University, Ottawa K1S 5B6, Canada*

Complete contact information is available at: https://pubs.acs.org/10.1021/acssensors.9b02155

Author Contributions

M. Loyez (writing, experiments, and data processing); E.M.H. (writing, aptamer selection, cell cultures, and experiments); M. Lobry (TFBG production and data processing); F.L. (TFBG

https://dx.doi.org/10.1021/acssensors.9b02155
ACS Sens. 2020, 5, 454−463

production and gold deposition, experiments); C.C. and R.W. (writing, supervision and project management, and coordination at the University of Mons, Belgium); W.G.W. and M.C.D. (supervision and project management at Carleton University, Canada). J.A. (writing, supervision, data analysis, and project coordination at Carleton University, Canada).

Funding

This work was financially supported by the Fonds de la Recherche Scientifique, FNRS under the FRIA Grant of Médéric Loyez (FRS-FNRS), the Associate Researcher position of Christophe Caucheteur (FRS-FNRS), and Grant no. O001518F (EOS-convention 30467715). The authors acknowledge the Natural Sciences and Research Council of Canada for their funding (Discovery Grant 224070).

Notes

The authors declare no competing financial interest.

■ ACKNOWLEDGMENTS

The authors kindly thank Albane Laronche for her dedicated work in the production of the optical fiber gratings and her precious help during the experiments. The authors also thank Mariel David for her help in the characterization of optical fiber signals. The authors warmly thank Rodney Aiton and Robert Vandusen for their high-quality gold evaporation process and AFM controls. The authors also thank the laboratory of Marine Biology of the University of Mons for access to the SEM equipment. Finally, the authors are grateful to the Anatoli Ianoul Research Group from Carleton University, especially to Daniel Prezgot for the AFM measurements.

■ REFERENCES

(1) Bray, F.; Ferlay, J.; Soerjomataram, I.; Siegel, R.; Torre, L. A.; Jemal, A. Global Cancer Statistics 2018: GLOBOCAN Estimates of Incidence and Mortality Worldwide for 36 Cancers in 185 Countries. *Ca-Cancer J. Clin.* **2018**, *68*, 394−424.

(2) Redig, A. J.; McAllister, S. S. Breast cancer as systemic disease: a view of metastasis. *J. Intern. Med.* **2013**, *274*, 113−126.

(3) Etayash, H.; Jiang, K.; Azmi, S.; Thundat, T.; Kaur, K. Real-Time Detection of Breast Cancer Cells Using Peptide- Functionalized Microcantilever Arrays. *Sci. Rep.* **2015**, *5*, No. 13967.

(4) De Mattos-Arruda, L.; Cortes, J.; Santarpia, L.; Vivancos, A.; Tabernero, J.; Reis-Filho, J. S. R.; Seoane, J. Circulating tumour cells and cell-free DNA as as tools for managing breast cancer. *Nat. Rev. Clin. Oncol.* **2013**, *10*, 377−389.

(5) Nagrath, S.; Sequist, L. V.; Maheswaran, S.; Bell, D. W.; Irimia, D.; Ulkus, L.; Smith, M. R.; Kwak, E. L.; Digumarthy, S.; Muzikansky, A.; Ryan, P.; Balis, U. J.; Tompkins, R. G.; Haber, D. A.; Toner, M. Isolation of rare circulating tumour cells in cancer patients by microchip technology. *Nature* **2007**, *450*, 1235−1239.

(6) Bidard, F.; Peeters, D. J.; Fehm, T.; Nolé, F.; Gisbert-Criado, R.; Mavroudis, D.; Grisanti, S.; Generali, D.; Garcia-Saenz, J. A.; Stebbing, J.; et al. Clinical validity of circulating tumour cells in patients with metastatic breast cancer: A pooled analysis of individual. *Lancet Oncol.* **2014**, *15*, 406−414.

(7) Zieglschmid, V.; Hollmann, C.; Böcher, O. Detection of disseminated tumor cells in peripheral blood. *Crit. Rev. Clin. Lab. Sci.* **2005**, *42*, 155−196.

(8) Sanders, M.; Lin, Y.; Wei, J.; Bono, T.; Lindquist, R. G. An enhanced LSPR fiber-optic nanoprobe for ultrasensitive detection of protein biomarkers. *Biosens. Bioelectron.* **2014**, *61*, 95−101.

(9) Masson, J. F. Surface Plasmon Resonance Clinical Biosensors for Medical Diagnostics. *ACS Sens.* **2017**, *2*, 16−30.

(10) Shevchenko, Y. Y.; Albert, J. Plasmon resonances in gold-coated tilted fiber Bragg gratings. *Opt. Lett.* **2007**, *32*, 211−213.

(11) Chiavaioli, F.; Baldini, F.; Tombelli, S.; Trono, C.; Giannetti, A. Biosensing with optical fiber gratings. *Nanophotonics* **2017**, *6*, 663−679.

(12) Wolfbeis, O. S. Fiber-Optic Chemical Sensors and Biosensors. *Anal. Chem.* **2004**, *76*, 3269−3284.

(13) Unser, S.; Bruzas, I.; He, J.; Sagle, L. Localized Surface Plasmon Resonance Biosensing: Current Challenges and Approaches. *Sensors* **2015**, *15*, 15684−15716.

(14) Guo, T. Fiber Grating-Assisted Surface Plasmon Resonance. *J. Lightwave Technol.* **2017**, *35*, 3323−3333.

(15) Caucheteur, C.; Guo, T.; Albert, J. Review of plasmonic fiber optic biochemical sensors: improving the limit of detection. *Anal. Bioanal. Chem.* **2015**, *407*, 3883−3897.

(16) Bandyopadhyay, S.; Biswas, P.; Chiavaioli, F.; Dey, T. K.; Basumallick, N.; Trono, C.; Giannetti, A.; Tombelli, S.; Baldini, F.; Bandyopadhyay, S. Long-period fiber grating: a specific design for biosensing applications. *Appl. Opt.* **2017**, *56*, 9846−9853.

(17) Pilla, P.; Trono, C.; Baldini, F.; Chiavaioli, F.; Giordano, M.; Cusano, A. Giant sensitivity of long period gratings in transition mode near the dispersion turning point: an integrated design approach. *Opt. Lett.* **2012**, *37*, 4152−4154.

(18) Albert, J.; Shao, L.; Caucheteur, C. Tilted fiber Bragg grating sensors. *Laser Photonics Rev.* **2013**, *7*, 83−108.

(19) Caucheteur, C.; Loyez, M.; González-Vila, Á.; Wattiez, R. Evaluation of gold layer configuration for plasmonic fiber grating biosensors. *Opt. Express* **2018**, *26*, 24154−24163.

(20) Lobry, M.; Lahem, D.; Loyez, M.; Debliquy, M.; Chah, K.; David, M.; Caucheteur, C. Non-enzymatic D-glucose plasmonic optical fiber grating biosensor. *Biosens. Bioelectron.* **2019**, *142*, No. 111506.

(21) Loyez, M.; Lobry, M.; Wattiez, R.; Caucheteur, C. Optical fiber gratings immunoassays. *Sensors* **2019**, *19*, 2595.

(22) Loyez, M.; Albert, J.; Caucheteur, C.; Wattiez, R. Cytokeratins biosensing using tilted fiber gratings. *Biosensors* **2018**, *8*, 74.

(23) Chiavaioli, F.; Zubiate, P.; Del Villar, I.; Zamarreño, C. R.; Giannetti, A.; Tombelli, S.; Trono, C.; Arregui, F. J.; Matias, I. R.; Baldini, F. Femtomolar detection by nanocoated fiber Label-Free Biosensors. *ACS Sens.* **2018**, *3*, 936−943.

(24) Guo, T.; González-Vila, Á.; Loyez, M.; Caucheteur, C. Plasmonic Optical Fiber-Grating Immunosensing: A Review. *Sensors* **2017**, *17*, 2732.

(25) Daems, D.; Delport, F.; Mariën, N.; Orbie, L.; Aernouts, B.; Adriaens, I.; Huybrechts, T.; Saeys, W.; Spasic, D.; Lammertyn, J. Competitive inhibition assay for the detection of progesterone in dairy milk using a fiber optic SPR biosensor. *Anal. Chim. Acta* **2016**, *950*, 1−6.

(26) Guo, T.; Liu, F.; Liang, X.; Qiu, X.; Huang, Y.; Xie, C.; Xu, P.; Mao, W.; Guan, B.-O.; Albert, J. Highly sensitive detection of urinary protein variations using tilted fiber grating sensors with plasmonic nanocoatings. *Biosens. Bioelectron.* **2016**, *78*, 221−228.

(27) Lu, J.; Spasic, D.; Delport, F.; Van Stappen, T.; Detrez, I.; Daems, D.; Vermeire, S.; Gils, A.; Lammertyn, J. Immunoassay for Detection of Infliximab in Whole Blood Using a Fiber-Optic SPR Biosensor. *Anal. Chem.* **2017**, *89*, 3664−3671.

(28) Loyez, M.; Larrieu, J.-C.; Chevineau, S.; Remmelink, M.; Leduc, D.; Bondue, B.; Lambert, P.; Devière, J.; Wattiez, R.; Caucheteur, C. *In situ* cancer diagnosis through online plasmonics. *Biosens. Bioelectron.* **2019**, *131*, 104−112.

(29) Ribaut, C.; Loyez, M.; Larrieu, J. C.; Chevineau, S.; Lambert, P.; Remmelink, M.; Wattiez, R.; Caucheteur, C. Cancer biomarker sensing using packaged plasmonic optical fiber gratings: Towards in vivo diagnosis. *Biosens. Bioelectron.* **2017**, *92*, 449−456.

(30) Hassan, E. M.; Willmore, W. G.; Mckay, B. C.; DeRosa, M. C. *In vitro* selections of mammaglobin A and mammaglobin B aptamers for the recognition of circulating breast tumor cells. *Sci. Rep.* **2017**, *7*, No. 14487.

(31) Zehentner, B. K.; Persing, D. H.; Deme, A.; Toure, P.; Hawes, S. E.; Brooks, L.; Feng, Q.; Hayes, D. C.; Critichlow, C. W.; Houghton, R. L.; Kiviat, N. B. Mammaglobin as a novel breast cancer

biomarker: multigene reverse transcription-PCR assay and sandwich ELISA. *Clin. Chem.* **2004**, *50*, 2069−2076.
(32) Galvis-jiménez, J. M.; Curtidor, H.; Patarroyo, M. A.; Monterrey, P.; Ramírez-clavijo, S. R. Mammaglobin peptide as a novel biomarker for breast cancer detection. *Cancer Biol. Ther.* **2013**, *14*, 327−332.
(33) Hassan, E. M.; Willmore, W. G.; DeRosa, M. C. Aptamers: Promising Tools for the Detection of Circulating Tumor Cells. *Nucleic Acid Ther.* **2016**, *26*, 335−337.
(34) Zhang, Y.; Lai, B. S.; Juhas, M. Recent Advances in Aptamer Discovery and Applications. *Molecules* **2019**, *24*, No. 941.
(35) Leblebici, P.; Leirs, K.; Spasic, D.; Lammertyn, J. Encoded particle microfluidic platform for rapid multiplexed screening and characterization of aptamers against influenza A nucleoprotein. *Anal. Chim. Acta* **2019**, *1053*, 70−80.
(36) Shevchenko, Y.; Francis, T. J.; Blair, D.; Walsh, R.; Derosa, M. C.; Albert, J. *In situ* biosensing with a surface plasmon resonance fiber grating aptasensor. *Anal. Chem.* **2011**, *83*, 7027−7034.
(37) Kosuri, S.; Church, G. M. Large-Scale de novo DNA synthesis: technologies and applications. *Nat. Methods* **2014**, *11*, 499−507.
(38) Chiavaioli, F.; Gouveia, C. A. J.; Jorge, P. A. S.; Baldini, F. Towards a uniform metrological assessment of grating-based optical fiber sensors: from refractometers to biosensors. *Biosensors* **2017**, *7*, No. 23.
(39) Lavín, Á.; de Vicente, J.; Holgado, M.; Laguna, M. F.; Casquel, R.; Santamaría, B.; Maigler, M. V.; Hernández, A. L.; Ramírez, Y. On the determination of uncertainty and limit of detection in label-free biosensors. *Sensors* **2018**, *18*, 2038.
(40) Feng, D.; Zhou, W.; Qiao, X.; Albert, J. High resolution fiber optic surface plasmon resonance sensors with single-sided gold coatings. *Opt. Express* **2016**, *24*, 16456−16464.
(41) Caucheteur, C.; Voisin, V.; Albert, J. Near-infrared grating-assisted SPR optical fiber sensors: design rules for ultimate refractometric sensitivity. *Opt. Express* **2015**, *23*, 2918−2932.
(42) Geltmeier, A.; Rinner, B.; Bade, D.; Meditz, K.; Witt, R.; Bicker, U.; Bludszuweit-Philipp, C.; Maier, P. Characterization of dynamic behaviour of MCF7 and MCF10A cells in ultrasonic field using modal and harmonic analysis. *PLoS One* **2015**, *10*, No. e0134999.
(43) Mateus, A.; Matsson, P.; Artursson, P. Rapid measurement of intracellular unbound drug concentrations. *Mol. Pharm.* **2013**, *10*, 2467−2478.
(44) Cennamo, N.; Pesavento, M.; Lunelli, L.; Vanzetti, L.; Pederzolli, C.; Zeni, L.; Pasquardini, L. An easy way to realize SPR aptasensor: A multimode plastic optical fiber platform for cancer biomarkers detection. *Talanta* **2015**, *140*, 88−95.
(45) Yanase, Y.; Hiragun, T.; Ishii, K.; Kawaguchi, T.; Yanase, T.; Kawai, M.; Sakamoto, K.; Hide, M. Surface plasmon resonance for cell-based clinical diagnosis. *Sensors* **2014**, *14*, 4948.
(46) Ogura, T.; Tanaka, Y.; Toyoda, H. Whole cell-based surface plasmon resonance measurement to assess binding of anti-TNF agents to transmembrane target. *Anal. Biochem.* **2016**, *508*, 73−77.
(47) Eustis, S.; El-Sayed, M. A. Why gold nanoparticles are more precious than pretty gold: Nobel metal surface plasmon resonance and its enhancement of the radiative and nonradiative properties of nanocrystals of different shapes. *Chem. Soc. Rev.* **2006**, *35*, 209−217.
(48) Yu, H.; Peng, Y.; Yang, Y.; Li, Z.-Y. Plasmon-enhanced light-matter interactions and applications. *npj Comput. Mater.* **2019**, *5*, No. 45.

https://dx.doi.org/10.1021/acssensors.9b02155
ACS Sens. 2020, 5, 454−463